Marine Geophysical Research (2019) 40:99–110
https://doi.org/10.1007/s11001-019-09381-x

ORIGINAL RESEARCH PAPER

Rift structures and its related unconformities on and adjacent the Dongsha Rise: insights into the nature of the high-velocity layer in the northern South China Sea

Chao Lei[1,2] · **Jianye Ren**[1] · **Xiong Pang**[3]

Received: 18 April 2018 / Accepted: 30 January 2019 / Published online: 6 February 2019

Abstract
It is curious that the typical feature of high-velocity layer (HVL) underneath the crust for the magma-rich margin was found in the magma-poor margin of the South China Sea. In order to better understand the nature and age of the HVL in the South China Sea, here we provide seismic imaging on the Cenozoic structure and sedimentation using a regional seismic reflection profile combined with existing drilling data and seismic refraction lines in the northeastern South China Sea. An important finding is that the extent of erosion since Neogene is only on the Dongsha Rise and is much smaller than that of the HVL observed across the northern margin of the South China Sea, which suggests the occurrence of the HVL has no influence on the erosion on Dongsha Rise through Neogene. On the regional seismic profiles, the different structures between the deepwater rifted margins and the continental shelf were also observed. The faults in the Zhuyi Sub-basins on the continental shelf are imaged to be high-angle and bound a series of grabens and horsts. In contrast, the deepwater region is characterized by tilted fault blocks and an array of listric normal faults, which extremely thinned the crust to be ~5–10 km. After middle Miocene, active magmatism occurred in the deepwater region at the time of post-spreading of oceanic crust. These listric faults on the hyper-extended crust is interpreted to be conduits for magma migration to the shallower levels. This typical structure in the deepwater region changed the geophysical nature of the HVL underneath the extreme thinned crust, which should be formed before the event of hyper-extension and is likely to be associated with the subduction of the paleo-Pacific toward the Asia in the late Cretaceous. Our study will answer the question why the South China Sea with the HVL underneath the crust is a magma-poor passive margin.

Keywords Passive margin · South China Sea · High-velocity layer · Hyper-extended crust · Magma-poor margin

Introduction

The high-velocity layer (HVL) at the base of lower crust was firstly observed in the magma-rich passive margin of the conjugate East Greenland-Vøring margin offshore Norway (Voss and Jokat 2007; and references therein), which is characterized by P-wave velocities (Vp) of 7.1 to 7.7 km/s and Vp/Vs ratios ranging between 1.8 and 1.9 (Mjelde et al. 2003; O'Reilly et al. 1996). There is no census for this "high velocity", but academic community usually regards the Vp value less than 7 km/s as normal and greater than that is HVL according to the Vp values of unaltered gabbroic oceanic crust (layer 3: 6.8–7.1 km/s after Mooney et al. 1998). In general, the HVL in the offshore Norway is usually thought to represent mafic intrusions related to the last phase of rifting (Mjelde et al. 2003) or retrograded and emplaced Caledonian eclogite (Gernigon et al. 2003).

The South China Sea is a marginal sea in the western Pacific region (Fig. 1), which developed hyper-extended crust adjacent to the ocean-continental boundary (Lei and Ren 2016; Lei et al. 2018; McIntosh et al. 2014; Savva et al. 2013). Deep seismic imaging reveal that the HVL occurs at the base of the lower crust of the northeastern South China

✉ Chao Lei
clei@cug.edu.cn

[1] Key Laboratory of Tectonics and Petroleum Resources of Ministry of Education, China University of Geosciences, Wuhan 430074, China

[2] College of Marine Science and Technology, China University of Geosciences, Wuhan 430074, China

[3] China National Offshore Oil Corporation Ltd., Shenzhen 518054, China

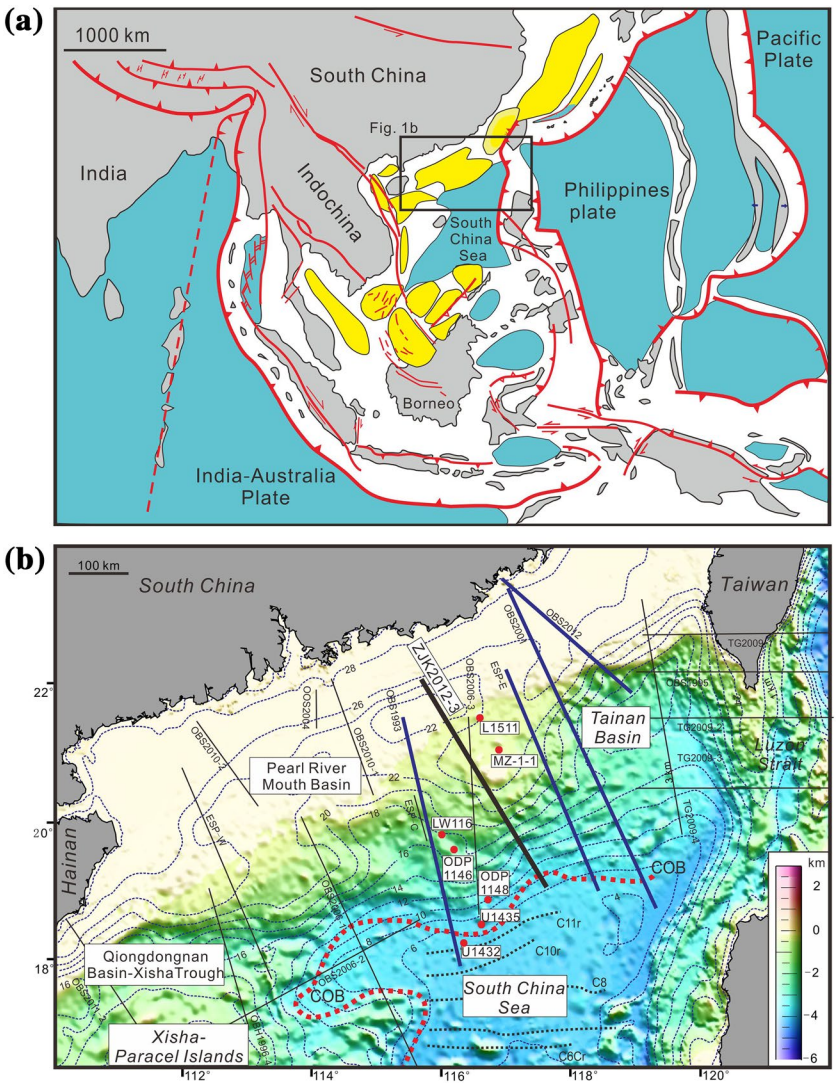

Fig. 1 **a** Tectonic map shows the locations of the northern South China Sea. **b** Bathymetric map of the northern South China Sea showing our regional seismic profile (black solid line) and drilling sites (red solid dots). Deep seismic refraction profiles released are shown in blue solid lines (Nissen et al. 1995; Wang et al. 2006; Yan et al. 2001; Wan et al. 2017). The red dash line, black solid lines and blue dash lines shows the continent-ocean boundary (COB) (Lei et al. 2018), magnetic anomaly lineation (Li et al. 2014) and crust thickness (Bai et al. 2015), respectively

Sea (Fig. 2) (Nissen et al. 1995; Wan et al. 2017; Wang et al. 2006; Yan et al. 2001; Zhao et al. 2010). It is curious that the HVL is usually observed in the magma-rich passive margin was imaged in the northeastern South China Sea, which has been widely suggested to be a magma-poor passive margin by the previous studies (Franke 2013; and the references therein). Their evidence is that seaward-dipping reflection was not imaged on the seismic profiles, which is one of the key characteristics diagnosed of volcanic-rich passive margin (Geoffroy 2005; and the reference therein). The HVL recognized in the northeastern South China Sea has a variable thickness and tends to thin or pinch out toward the continent-oceanic crust (Figs. 1, 2). Overall, on the continental shelf a ~ 4–7 km thick HVL (~ 7.0–7.6 km/s) occurred at the base of lower crust, and the thickness of HVL on the continental slope decrease to be ~ 2–3 km thick (Fig. 2).

This study presents a new regional multichannel seismic profile across the continental shelf, slope and oceanic crust in the northeastern South China Sea. We aim to decipher the structure and sedimentary filling pattern overlying the crust with the HVL, which highlights importance of the detachment faulting and associated magma addition in the deepwater region during the evolution of the passive margin.

Geological and tectonic setting

The South China Sea with an area of almost 300 km^2 represent one of the largest marginal seas worldwide (Fig. 1). To the west of the oceanic crust of the South China Sea, it is the Eastern Vietnamese strike-slip fault, which is suggested to be connected with the Red River Fault to the SE margin of the Tibetan Plateau (Morley 2002; Briais et al. 1993; Sun et al. 2003). To the South of the oceanic crust, a trough occurred to the north of the Borneo island as result of the collision between the Borneo and Nansha blocks (Hall 2002). To the east of the oceanic crust, it is the Manila Trench resulted from the subduction of the

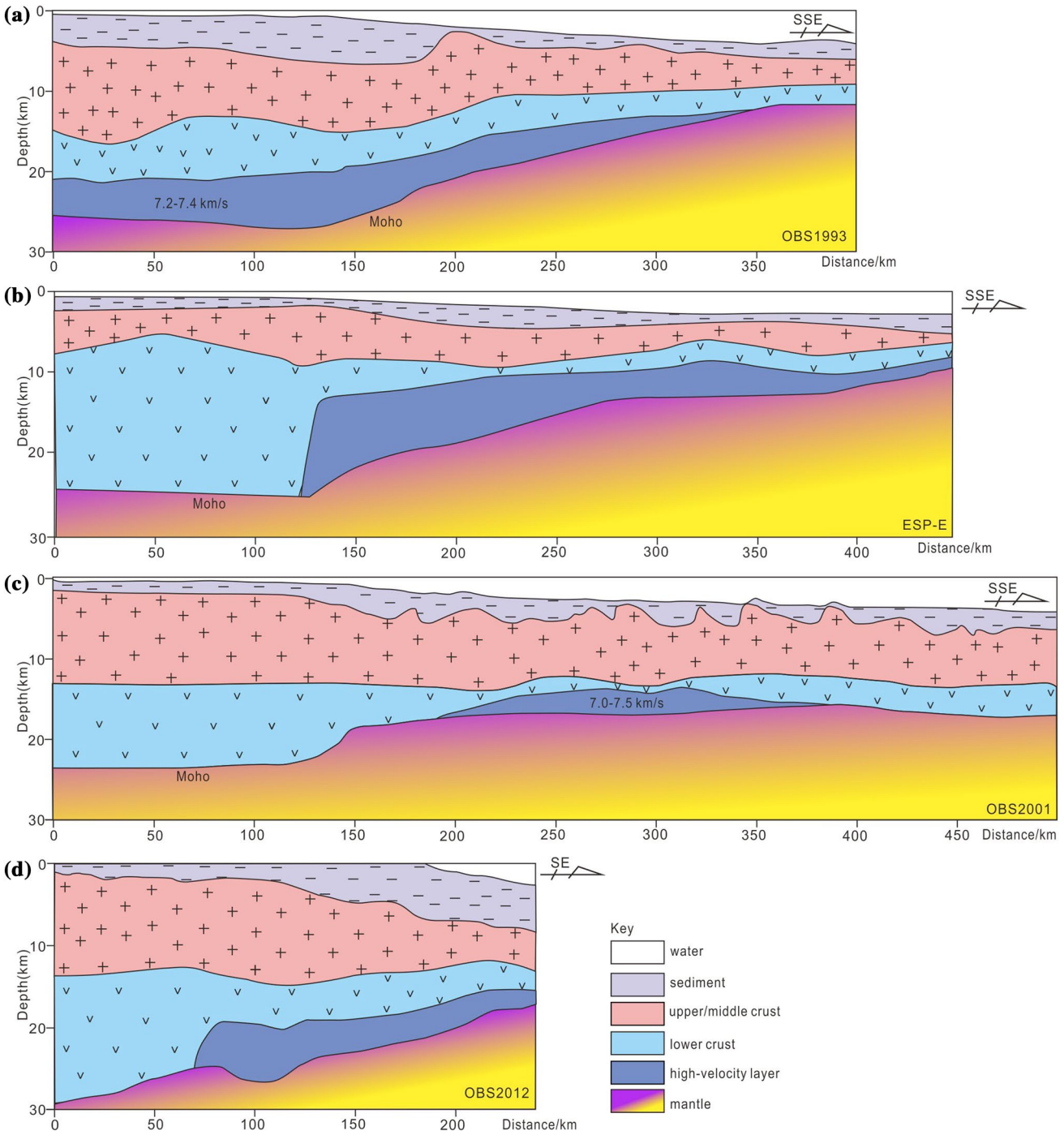

Fig. 2 Deep seismic refraction profiles present the crust structure in the northern South China Sea (Nissen et al. 1995; Wan et al. 2017; Wang et al. 2006; Yan et al. 2001). Note the locations of these profiles are illustrated by blue solid lines in Fig. 1b

lithosphere of the South China Sea toward the Luzon arc (Eakin et al. 2014). To the north of the oceanic crust, it is the Pearl River Mouth Basin and Xisha Trough with hyper-extended crust in the distal margin (Gao et al. 2016; Lei and Ren 2016; Lei et al. 2018).

The South China Sea is underlain by the oceanic crust and is believed to result from continental extension, continental breakup and subsequent oceanic spreading (Li et al. 2014; Sibuet et al. 2016). Before extension, the area of the South China Sea is along the arc of an Andean-style Mesozoic

subduction zone (Li and Li 2007; Zhou et al. 2008). After subduction, continental extension started in the late Cretaceous-early Paleocene (Ru and Pigott 1986) and has a new phase of distributed continental rifting during Eocene–Oligocene. The continued rifting thinned the crust and lastly produced the opening of the South China Sea (Cullen 2010; Hall 2002; Pubellier and Meresse 2013). The latest studies show that the seafloor spreading was unraveled to have started at ~ 33 Ma and ceased at ~ 16.5 Ma, which is estimated based on magnetic anomalies and have yet to be confirmed by in situ sampling of the deep sediments at the IODP sites (Koppers and Expedition 2014; Li et al. 2014), which is almost similar to the age from geophysical magnetic data (Briais et al. 1993).

The Pearl River Mouth Basin is one of the largest and petroliferous Cenozoic basin in the South China Sea (Fig. 1) (Pang et al. 2007; Lei et al. 2018), which covers more than ten sub-basins and structural highs. To the north, it is the South China on which the Pearl River catchment situates. To the East and west, islands of Taiwan and Hainan bound the basin, respectively. To the South, it is the oceanic crust of the South China Sea, whose nature is recognized and determined by marine magnetic data (Fig. 1) (Briais et al. 1993; Li et al. 2014).

Dataset and methodology

In this study a regional seismic profile imaging the continental shelf, slope and oceanic crust is examined (Fig. 1b), coincident with previous local seismic profiles and drilling data from ODP/IODP expeditions and petroleum exploration. In the last decades, CNOOC acquired a ~ 430 km long regional seismic reflection profile (ZJK2012-3), which crosses the eastern segment of the Pearl River Mouth (Fig. 1b). This transect has high quality recording to a depth of 8 s two way travel-time (TWT) and offers a much improved image of the northern South China Sea. Available academic (ODP/IODP sites) and industrial drilling data were considered in our study (Fig. 1b). We chose those wells that penetrated Paleogene sediments to make the borehole descriptions, e.g. ODP site 1148 (Fig. 3).

In our study, interpretation of seismic sequences and structures on the seismic profiles were performed using Geoframe software. The ages of regional stratigraphic horizons were after the previous research results from petroleum exploration drilling sites (Pang et al. 2007), as well as ODP drilling site 1148 (Wang et al. 2000) and IODP drilling site U1435 in the deepwater region (Li et al. 2014). Based on the amplitude and the reflection configuration, as well as the geometry of various seismic bodies, in accordance to the method of contact relations and internal and external configurations (Mitchum et al. 1977; Posamentier and Vail 1988; Van Wagoner et al. 1988), the Cenozoic succession in the basin was divided into four seismic units (Units A, B, C and D) and seven seismic sub-units in this study (Fig. 3). The seismic character, spatial distribution, and internal geometry of the four units have been described in detail in the local Sub-basins and/or structural highs (Pang et al. 2007; Sun et al. 2017; Zhao et al. 2018). Each unit is bounded at the base or top by a significant unconformity.

Result

Rift structure and fault style

The profile ZJK2012-3 images the structure on and adjacent Dongsha Rise (Figs. 1b, 4). The crust is presented to be cut by the faults where they bounds a series of accommodation for the Cenozoic sediment, e.g. Zhuyi and Jinghai Sub-basins (Fig. 4), where the Cenozoic sediments are estimated to be at least 6.5 km (3.5 s TWT) and 5.8 km (3.3 s TWT), respectively. The Zhuyi Sub-basins is located on the continental shelf, which is bounded by a series of high-angle normal faults, e.g. Faults N3, N4 and N5 (Figs. 4, 5a). Theses faults are active prior to the time of formation of Horizon T60 dated at 23.8 Ma. Their heaves are estimated to ~ 3–5 km. In contrast, faults cut all the Cenozoic sediment on the Dongsha Rise, where the thickness of sediments deposited on the hanging wall of the faults since middle Miocene is same as that on the footwall. Overlying the reflector T32, the sediment thickness of each sub-units shows obvious change across the faults (Fig. 4). This contrast sedimentary characteristics across the faults indicates that faulting on the Dongsha Rise occurred since Middle Miocene.

The Cenozoic sediments on the Dongsha Rise are estimated to be at most 0.8 km (0.9 s TWT) (Fig. 4), which are much thinner than the sediment trapped in the Zhuyi Sub-basins on the shelf and Jinghai Sub-basin in the deepwater region. All of this thinner Cenozoic sedimentary strata on the Dongsha Rise is dated to be deposited during the post-rift stage by the seismic stratigraphy. Underlying uniform thickness of the sediments we did not observe prominent syn-rift sediments. The lack of syn-rift sediment on the Dongsha Rise has also been indicated by the borehole data of Well MZ-1-1. Likewise, the post-rift sediments were directly deposited on the pre-Cenozoic rocks (Fig. 4). At the distance of ~ 250 km on the profile ZJK2012-3, the sediments dated to be deposited during Mesozoic age were observed to be angular unconformity with its overlying Cenozoic sediment (Figs. 4, 6a). It is noteworthy that although the faults here are much smaller (Figs. 4, 7), they are active at the present-day as the crystalline basement and overlying sediments was cut and deformed by the faulting.

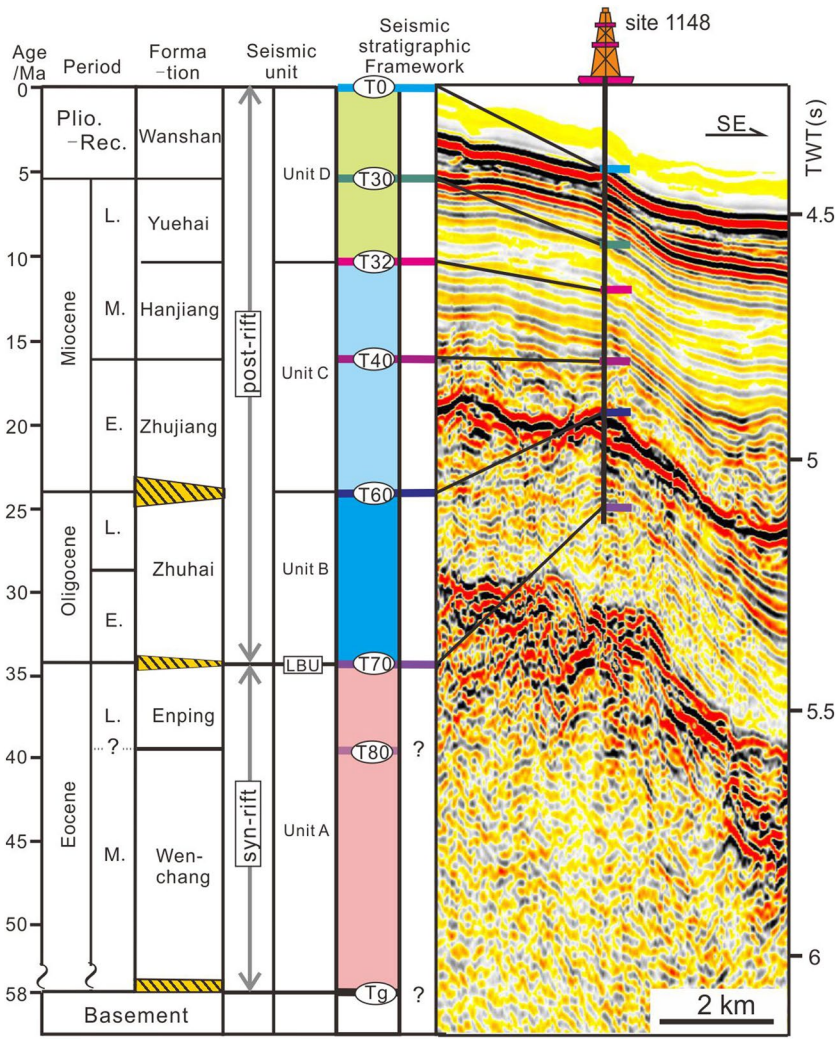

Fig. 3 Seismic stratigraphy framewrok and seismic units used in this study are present alongside seismic profile constrained by ODP site 1148. *LBU* Lithospheric breakup unconformity (Lei et al. 2018)

Fig. 4 **a** Uninterpreted and **b** interpreted regional seismic reflection profile across the Dongsha Rise and adjacent area (location shown in Fig. 1b). Magmatic structure S47 is after Lei et al. (2018)

Jinghai Sub-basin is located in the deepwater region (Fig. 4). The faults bounded the Sub-basin (faults N1 and N2) are imaged to cut the basement, which was displaced by ~ 18 km wide. The boundary faults, e.g. Faults N1 and N2, separate Cenozoic sediments from crystalline basement. At the level of deep domain the faults have small dips. Theses faults propagated upward and is presented to be larger dips where they offset Oligocene stratigraphy (Fig. 4). The fault N1 dips toward north and the fault N2 dips toward south. A structural high in the center of the Jinghai Sub-basin is

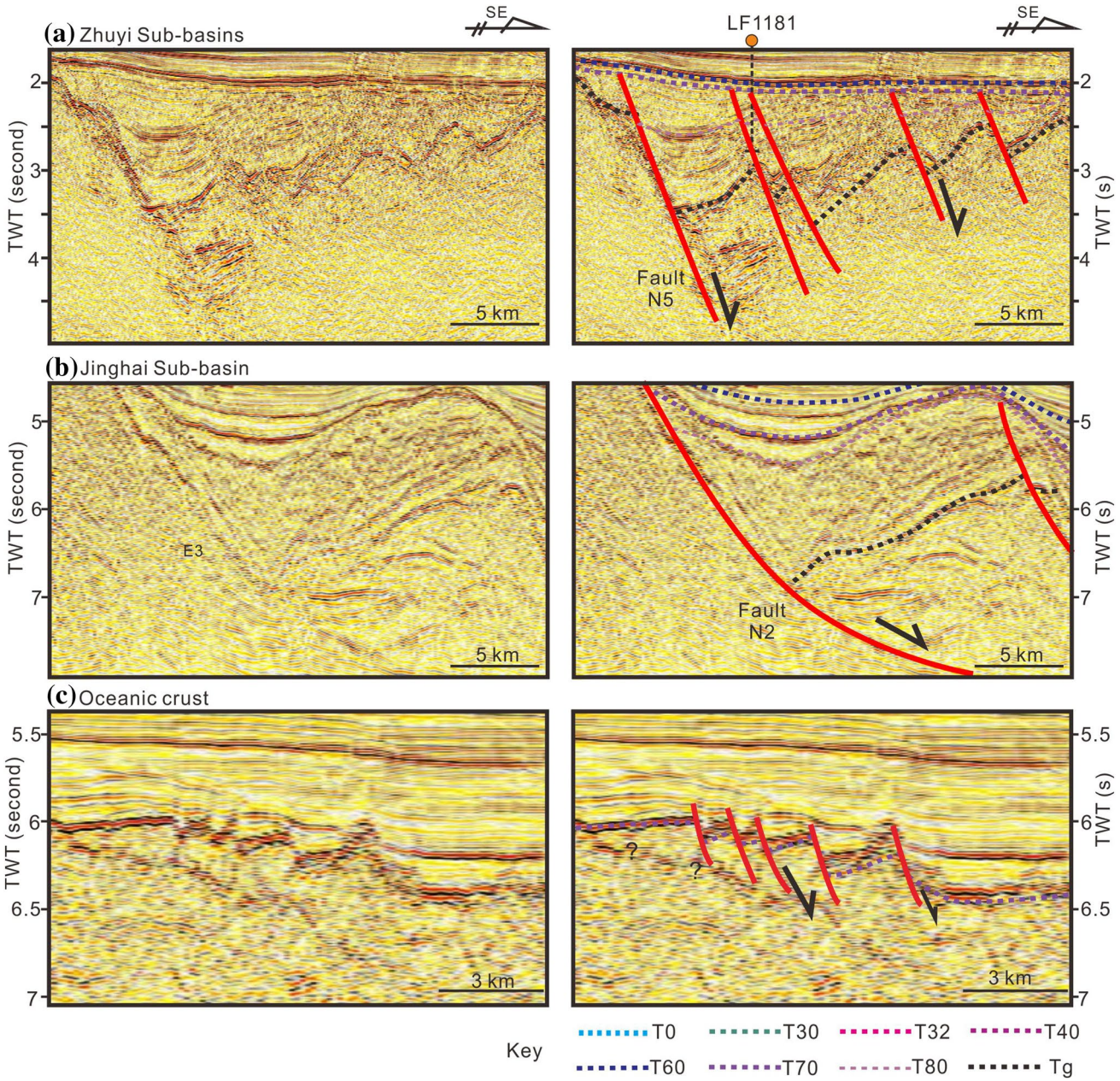

Fig. 5 Close-up images from the seismic profile ZJK2012-3 presenting the fault styles on the Zhuyi Sub-basins (**a**), Xingning Sub-basin (**b**) and oceanic crust (**c**), respectively

bounded by faults N1 and N2. The seismic refection of the structural high shows that within the body there are likely magmatic diapir (Figs. 4, 8). Contact and complex curving boundaries between the sediment and the diapiric structure were imaged on the seismic profile (Fig. 8). On the top of this diapirc structure, two extrusive structures were observed (Fig. 8). Additionally, the thickest Cenozoic sediment accumulation is located on the hanging walls of the boundary faults N1 and N2, and is estimated to be as much as ~ 5.8 km (~ 3.3 s TWT). To the South of Jinghai Sub-basin is the oceanic crust (Fig. 4). The faults there are much smaller than that in the Jinghai Sub-basin (Figs. 4, 5c).

Seismic horizons and sediment units

Syn-rift megasequence

The Cenozoic sediments imaged on the seismic profile can be divided into units A, B, C and D according to their prominent sequence boundaries (Figs. 3, 4). The Units A bounded

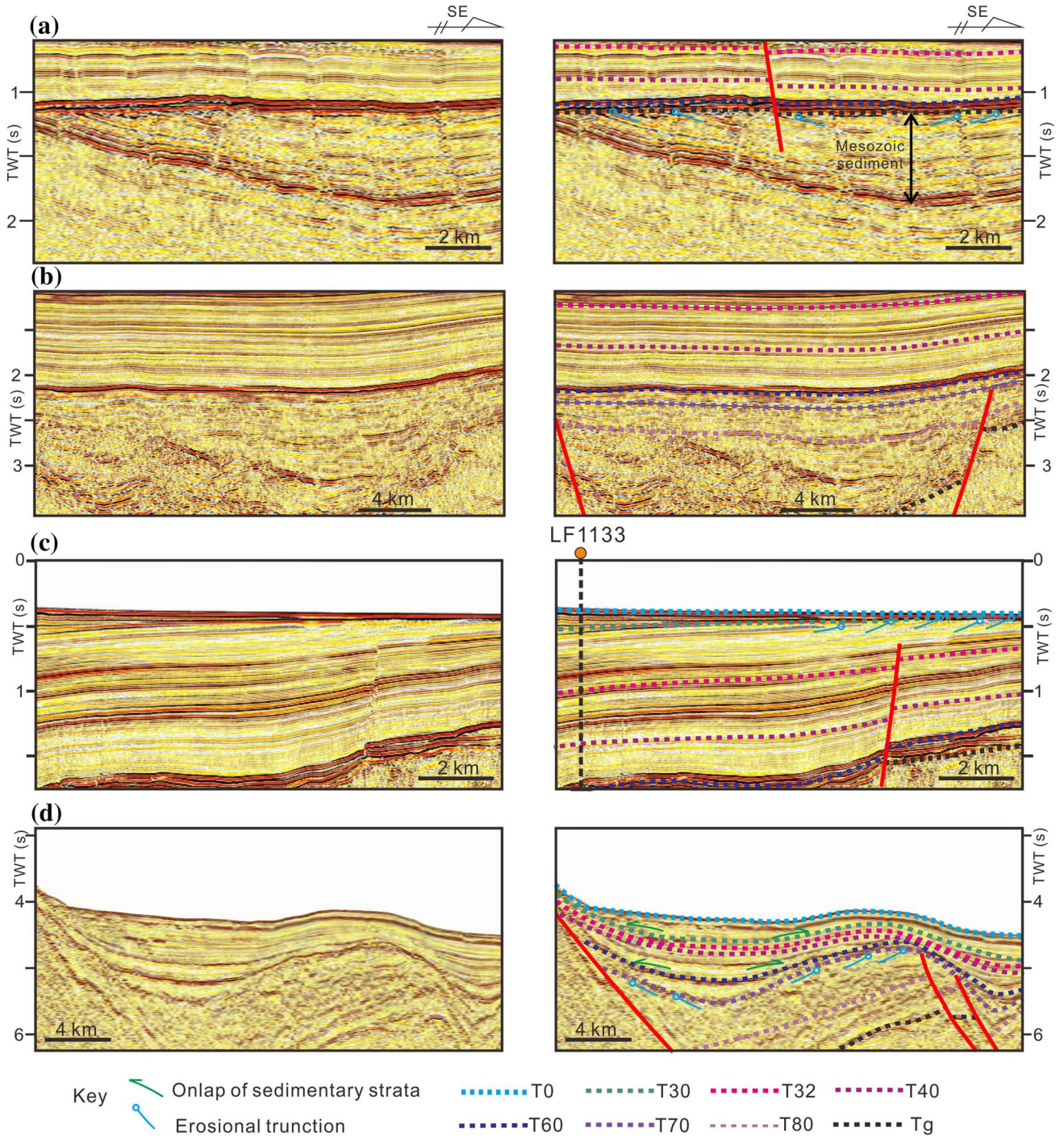

Fig. 6 Close-up images from the seismic profile ZJK2012-3 show prominent seismic reflection characteristics. **a** Horizon Tg truncates the Mesozoic sediment; **b** horizons T80, T70 and T60 are highlighted; **c** the sediments overlying the T32 are eroded by the uplift of the Dongsha Rise; **d** the post-rift sediment was not strongly faulted in the Jinghai Sub-basin

by the reflectors Tg and T70, which is defined to be syn-rift sediment deposited at the time between onset of rifting and onset of steady sate seafloor spearding at ~ 33 Ma. Reflector Tg is the deepest traceable surface within the sediments and is presented to be an regional unconfomity with high-amplitude characteristics (Figs. 4, 6). However, the reflector Tg is faulted by the high angle faults in the Zhuyi Sub-basins, small-scale faults in Dongsha Rise and listrical faults in the Jinghai Sub-basin (Figs. 4, 5a, b, 7). The depth of the Reflector Tg shows the topographic feature of the

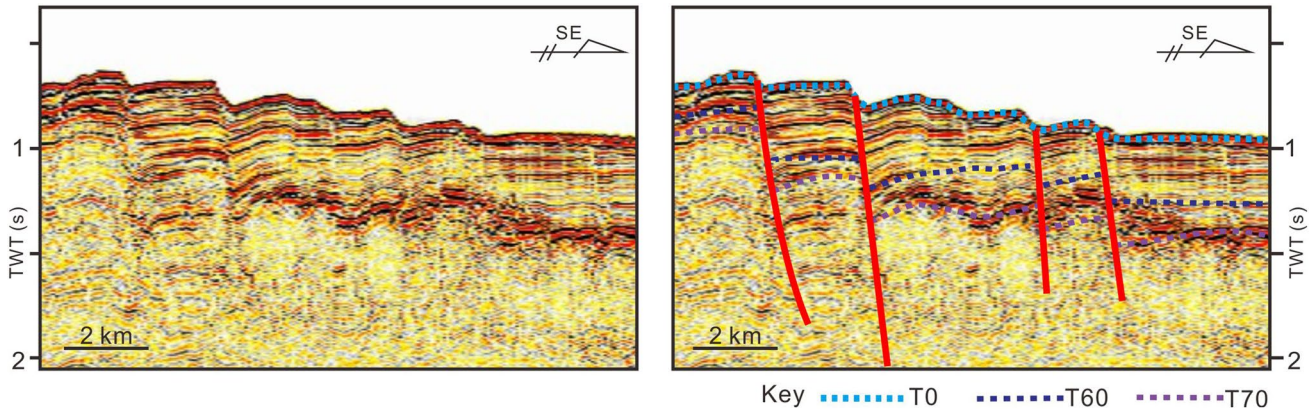

Fig. 7 Close-up images from the seismic profile ZJK2012-3 presenting strongly faulting on the Dongsha Rise, where the faults cut through all the sediments with large fault heave

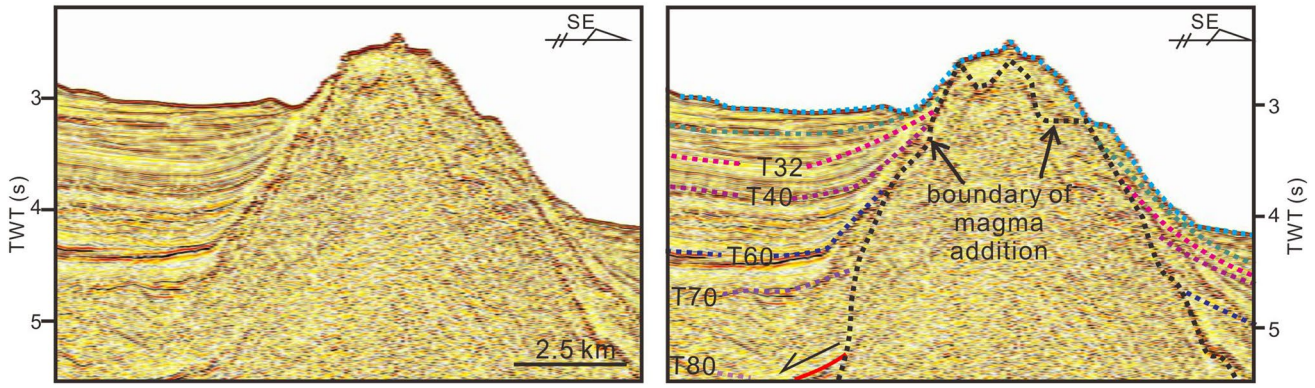

Fig. 8 Close-up images from the seismic profile ZJK2012-3 presenting magmatic structure in the Jinghai Sub-basin

crystalline basement, which indicates the Dongsha Rise has much smaller basement subsidence relative to those of the Zhuyi Sub-basins to the north and the Jinghai Sub-basin to the South (Fig. 4). Underlying the reflector Tg is the acoustic basement of the Cenozoic basin. However, on the Dongsha Rise the geological body underlying reflector Tg is imaged to be continous reflection (Fig. 6a), which is contrained to be pre-Cenozoic sediment penetrated by the MZ-1-1 (Li et al. 2008).

Reflector T70 is another prominent seismic unconformity on the top of the Unit A (Fig. 4), which separates the syn-rift and post-rift sedimentary packages (Fig. 3). It is imaged to be merged with its overlying Reflector T60 in the areas of North Massif and Dongsha Rise (Fig. 4), where they generates a conformable surface. At the depocenters of Zhuyi and Jinghai Sub-basins, the reflector T70 is present to be parallel character with its adjacent horizons, e.g. reflectors T80 and T60 (Fig. 6b, d).

Within the syn-rift sedimentary package, a distinct uncorformity with high seismic amplitude is observed, which separates the Unit A into two sub-units A1 and A2 (Fig. 6b, d). The Unit A1 on the continental shelf and slope is almost with similar wedge-geometry. The petroleum exploration drilling well LF1181 have penetrated the Unit A2, which shows this unit consists of interbed sandstone and shalestone. In contrast, the scale and thickness of the Unit A2 are imaged to be different across the margin. The thickness of the Unit A2 on the continental shelf is much thinner than that in the Jinghai Sub-basin (Fig. 5a, b), although the continental shelf is close to the sediment source of the South China. On the Dongsha Rise, zero thickness of the Unit A was observed. Internally, Unit A2 in the Zhuyi Sub-basins is characteristics of homogenous amplitude and continuous seismic reflections, which indicates that deposition there was uniform (Fig. 5a). However, Unit A2 in the Jinghai Sub-basin is dominated by variable amplitude and continuous reflections, which onlaps its underlying Reflector T80 (Fig. 5b). The Unit A2 can be correlated with upper part of the Unit II at IODP site U1435 (Li et al. 2014), which consists of sandstone deposited in deepwater environment. On the continental shelf in the Pearl River Mouth Basin, the Unit

A2 is composed of sands deposited in shallow water environment (Pang et al. 2007).

Post-rift megasequence

Post-rift megasequence overlies the continental breakup uncorformity T70 (Fig. 3). Overlying this reflector, strong faulting did not exist there. The grabens and hosrsts formed during syn-rift stage were covered by these post-rift sediments on the seismic profiles (Fig. 4). However, the faults on the Dongsha Rise continue to be active and cut the sediment, most of which even penetrate the seafloor and form faulted scarpments (Fig. 7).

On the seismic profile, seismic reflectors T60, T32 and T0 with strong amplitude and good-continuity are distributed across the margin, which separates the syn-rift sedimentary package into Units B, C and D (Fig. 4). Unit B consist of the Zhuhai Formation, which represents the oldest post-rift sediment across the margin (Fig. 3). Different with the distributed isolated depocenter of the Unit A, the extent of the Unit B is much larger and can be observed across the whole profile (Fig. 4). The Unit C, overlying the Unit B, is also well recognized across the margin with the exception of the southern part of the Dongsha Rise, where the Unit B was eroded and formed a prominent reflector T32 (Figs. 4, 6c). Underlying the reflector T32 the reflection is presented to be variable amplitude, moderate to good-continuity and parallel reflections (Fig. 4), which suggested that there was no active faults developed when this depostion occurred there.

Overlying the reflector T32, the sedimentary package is Unit D (Figs. 3, 4). Within the Unit D, several prominent unconformities with characteristics of trunction reflection are observed across the profile, especially on the Dongsha Rise (Figs. 4, 6c). The reflector T32 on the Dongsha Rise is firstly shown to be eroded by its overlying unconformities, which forms an angular unconformity (Fig. 4). The characteristics of angular uncorformities can be also observed at the reflector T0 on the Dongsha Rise (Fig. 4). In contrast, the post-rift sediments in the Jinghai Sub-basin, we did not observe any regional erosion (Fig. 4). The drift geometry in the Jinghai Sub-basin was observed, which consists of clay and was suggested to be contourite (Fig. 9) by the ODP Expedtion 184 (Wang et al. 2000). This contourite indicates it was deepwater setting at the time of erosion on the Dongsha Rise since Middle Micoene.

Strong erosion on the Dongsha Rise

Based on the regional seismic profile ZJK2012-3, the maximum thickness of the Cenozoic sediments in the Zhuyi Sub-basins, Dongsha Rise and Jinghai Sub-basin are estimated 6.5 km (3.5 s TWT), 0.8 km (0.9 s TWT) and 5.8 km (3.3 s TWT), respectively. On the Dongsha Rise the seismic boundary between Upper and Middle Miocene, i.e. horizon T32, is represent to be a prominent angular unconformity, which truncated its lower seismic Units A, B and C (Figs. 4, 6c). The remnant sedimentary package of the Units A, B and C varies considerably. The eroded sediment is estimated to be larger on the Dongsha Rise, and decreased toward the Zhuyi Sub-basins to the north and Jinghai Sub-basin to the south, respectively (Fig. 4). Erosion decreases more abruptly across the transiton between the Jinghai Sub-basin and Dongsha Rise (Fig. 4). In the Jinghai Sub-basin, we did not observe any seismic reflections indicating for erosion.

Discussion

No marginal scale erosion through Neogene: implication for the formation of HVL at least before Neogene

The HVL in the northeastern South China Sea occurred underneath the lower crust and stretches from the shelf to ocean-continental boundary. The extent of the HVL covers the Dongsha Rise and surrounding areas (Wang et al. 2006; Yan et al. 2001; Wan et al. 2017), which is estimated to be at least located underneath the crust of the Dongsha Rise, and Jinghai Rise. Because of isostatic rebound, magma underplating the crust will trigger the uplift of continental block

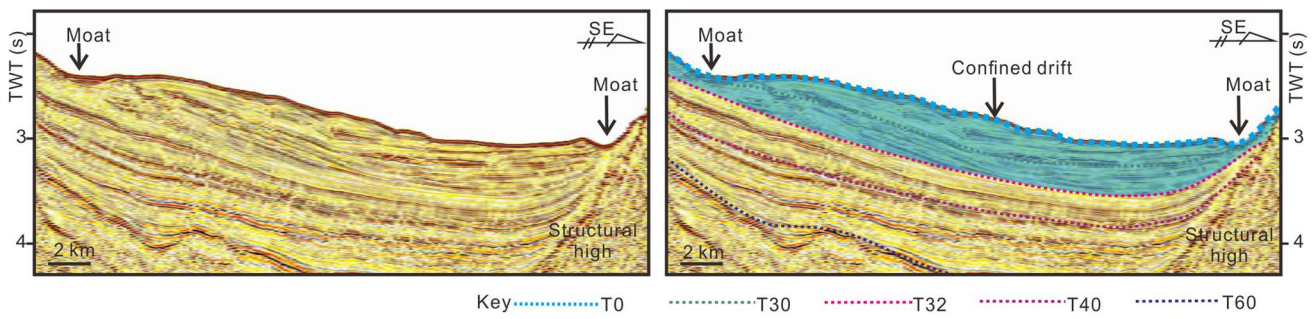

Fig. 9 Seamount and related contourite sedimentary system, including the moat and confined drift

and the production of the eroded sediment. However, exception of Dongsha Rise, we did not observe any strong erosion for the sedimentary succession to the south of the Dongsha Rise. In the Jinghai Sub-Basin, prolonged basement subsidence occurred in the Jinghai Sub-basin and its surrounding area (Lei et al. 2018). This sedimentation difference between the Dongsha Rise and Jinghai Sub-basin is possibly resulted from the subducting of the lithosphere of South China Sea toward the Luzon arc since Middle Miocene (Huang et al. 2012; and references therein). This event resulted into the uplift and associated erosion of the Dongsha Rise according to the numerical modeling (Lester et al. 2012). Dongsha Rise is at the forebulge tectonic unit associated with the subduction of the South China Sea lithosphere toward the Luzon arc. Therefore, the extent of the erosion is limited in the Dongsha Rise. The contribution of the HVL to form the erosion on the Dongsha Rise has been exaggerated. The process of the lithosphere of the South China Sea subducted toward the Luzon arc should be needed more detail research work at the transitional zone between Luzon arc and Dongsha Rise.

Mechanism for the formation of the HVL

The nature and origin of the HVL in the northeastern South China Sea are still controversial and probably more complex. Seismic surveys imaged HVL at the base of the crust to be characterized by Vp/Vs ratios of 1.76–1.94 (average 1.85) and the P-wave velocity of 7.0–7.5 km/s (Zhao et al. 2010). This HVL was interpreted to be from mafic magma underplating the lower crust in the northern margin of the South China Sea, which was related to the subduction of the Pacific plate toward the South China block since late Mesozoic (Li and Li 2007; Yan et al. 2001). In this case, the magma underplating the lower crust should have the homogeneous geology and geophysical characteristics from the continental shelf to the distal margin. However, the northern Dongsha Rise exhibits a higher magnetic anomaly zone than that in its surrounding area (Fig. 10), which was interpreted to be two tectonic parts by Wan et al. (2017). These characteristics indicates a tectonic boundary occurred between the shelf and the deepwater region.

The seismic profile ZJK2012-3 in our study shows the difference of the fault style on the continental shelf (Dongsha Rise) and slope (Jinghai Sub-basin). Different with the faults cutting the upper crust only on the slope, the low-angle faults was imaged to be sole into the lower crust at the slope of the northern South China Sea. Because of the occurrence of the low-angle faults in the Jinghai Sub-basin, the hyper-extended crust with thickness of 6–10 km were observed there (Lei et al. 2018). The places with this kind of extreme thinned crust, detachment faults may facilitate serpentinization of the underlying upper mantle and subsequent exhumation to the seafloor, which has been proven in the Iberian margin and the Alps (e.g. Manatschal 2004; Manatschal and Nievergelt 1997; Perez-Gussinye and Reston 2001; Whitmarsh and White 1996). Depending on the degree of serpentinization, the previous lab study show the Vp and densities was estimated to decreased at the range of 7.1–7.6 km/s observed underneath the lower crust. Underneath the Porcupine Basin, serpentinized mantle has been imaged to be underneath this extremely thinned crystalline crust (Reston and Morgan 2004; Prada et al. 2017).

However, a comparison with the distal parts of magma-poor margin of Iberian was not easily supported by the data observed in the northern South China Sea. Low Vp/Vs ratios (1.76–1.94) was observed in the northern South China Sea

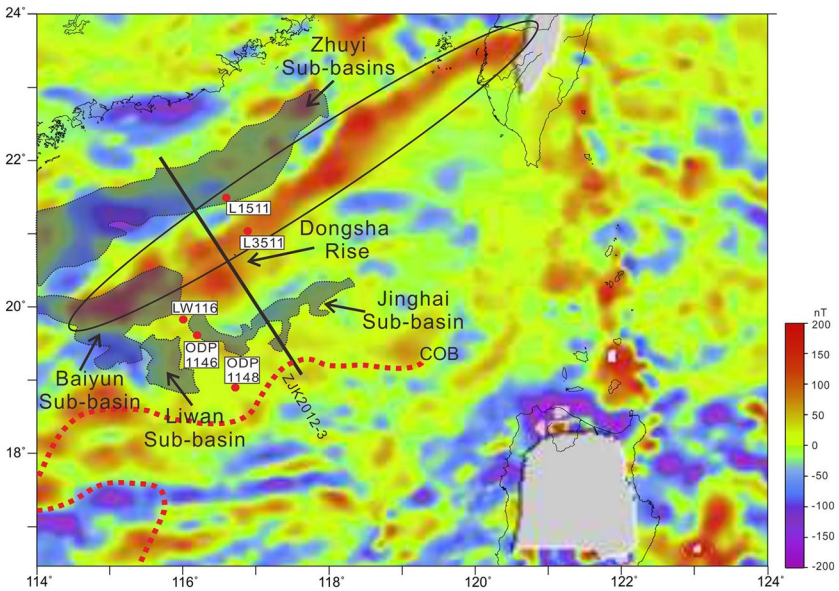

Fig. 10 High magnetic anomaly belt highlighted by black ellipse in the northern margin of the South China Sea. Magnetic data are after Wan et al. (2017)

(Zhao et al. 2010), which suggests the HVL consists of mafic composition. However, these low value of Vp/Vs ratios is an anverage Vp velocity vaule for the whole HVL, and we can not exclude other compostion occurred there. For example, the HVL is with mafic compostion, however mixed with serpentinized peridoties. In addtion, a serial of the magmic structure intruded or extruded the Cenozoic sedimentary succession in the northern South China Sea, especailly in the deepwater region (Lei et al. 2018; Fan et al. 2017). Their distribution is much smaller than the extent of the HVL observed on the seismic refraction profiles (Fig. 2). These magma additions in the deepwater region of South China Sea has been proposed for accretion models of igneous crust in the context of ridges with faster spreading rates of South China Sea than that in the Iberia margin after deepwater drilling of the Expeditions 367 and 368 in the central segment of the Pearl River Mouth Basin (Larsen et al. 2018). At the processes for the magma migrated from the deep domain into the sedimentary succession, the detachment faults was the most possible conduits for this transportation. And the water overlying the hyper-extended crust was easily penetrated into the mantle through the low-angle faults sole into the Moho. Therefore, the HVL underlying the hyper-extended crust in the deepwate region represent different characteristic with that on the Dongsha Rise, which resulted into the formation of the different tectonic parts in and around Dongsha Rise.

Conclusion

Our data presents new constraints on the basin structures and sedimentation in the deepwater margin and on the continental shelf of the South China Sea. The faults in the Zhuyi Sub-basins on the continental shelf are imaged to be high-angle, which bounded a series of grabens and horsts. The faults there was active at the stage of Eocene-early Oligocene. Contrary to the uniform thickness ~ 20–32 km of crust on the continental shelf, it is visible that the continental crust was abruptly thinned beneath the Jinghai Sub-basin, where it is characterized by an array of tilted fault blocks and an array of listric normal faults soling into the Moho. These low-angle faults and hyper-extended crust in the Jinghai Sub-basin indicate that extremely thinning occurred in the South China Sea is similar to the well-studied Iberian margin in the North Atlantic. The low-angle faults on the extreme thinned crust was likely to provide conduit for the magmatic migration into the sedimentary cover in the Jinghai Sub-basin. The hyper-extension changed the nature of the HVL underneath the crust in the deepwater region. However, the HVL on the contienntal shelf was not affected as result of lack of this detachment faults and associated extreme thinned crust. Therefore, the two tectonic zones of the HVL distinguished from magnetic anomaly were indicated to be formed after the occurrence of hyper-extended crust in the Oligocene.

Acknowledgements CNOOC, Beijing and Shenzhen are thanked for making their seismic and drilling data available. Funding for this work came from National Key Research and Development Project (2017YFC1405502), National Program on Global Change and Air-Sea Interaction (GASI-GEOGE-02), Natural Science Foundation of China (Nos. 41772093, 41830537, 91528301), and National Science and Technology Major Project of the Ministry of Science and Technology of China (2016ZX005008-001-001). We thank Hesheng Shi from CNOOC for useful comments and suggestions that improved the paper.

References

Bai Y et al (2015) Full-fit reconstruction of the South China Sea conjugate margins. Tectonophysics 661:121–135

Briais A, Patriat P, Tapponnier P (1993) Updated interpretation of magnetic anomalies and seafloor spreading stages in the South China sea: implications for the tertiary tectonics of Southeast Asia. J Geophys Res 98(B4):6299–6328

Cullen ARPH (2010) Rifting of the South China Sea: new perspectives. Pet Geosci 16(3):273–282

Eakin DH et al (2014) Crustal-scale seismic profiles across the Manila subduction zone: the transition from intraoceanic subduction to incipient collision. J Geophys Res 119(1):1–17

Fan C et al (2017) New insights into the magmatism in the northern margin of the South China Sea: spatial features and volume of intraplate seamounts. Geochem Geophys Geosyst 18(6):2216–2239

Franke D (2013) Rifting, lithosphere breakup and volcanism: comparison of magma-poor and volcanic rifted margins. Mar Pet Geol 43:63–87

Gao J et al (2016) Crustal structure and extension mode in the northwestern margin of the South China Sea. Geochem Geophys Geosyst. https://doi.org/10.1002/2016GC006247

Geoffroy L (2005) Volcanic passive margins. CR Geosci 337(16):1395–1408

Gernigon L, Ringenbach JC, Planke S, Le Gall B, Jonquet-Kolsto H (2003) Extension, crustal structure and magmatism at the outer Voring Basin, Norwegian margin. J Geol Soc 160(2):197–208

Hall R (2002) Cenozoic geological and plate tectonic evolution of SE Asia and the SW Pacific: computer-based reconstructions, model and animations. J Asian Earth Sci 20(4):353–431

Huang CY, Yi Y, Zhao QH, Lin CT (2012) Cenozoic stratigraphy of Taiwan: Window into rifting, stratigraphy and paleoceanography of South China Sea. Sci Bull 57(24):3130–3149

Koppers AAP, Expedition S (2014) On the 40Ar/39Ar dating of low-potassium ocean crust basalt from IODP Expediton 349, South China Sea, Abstract T31E-03 Presented at 2014. Fall Meeting, AGU, San Francisco

Larsen HC et al (2018) Rapid transition from continental breakup to igneous oceanic crust in the South China Sea. Nat Geosci 11(10):782–789

Lei C, Ren J (2016) Hyper-extended rift systems in the Xisha Trough: implications for extreme crustal thinning ahead of a propagating ocean of the South China Sea. Mar Pet Geol 77:846–864

Lei C, Ren J, Pang X, Chao P, Han X (2018) Continental rifting and sediment infill in the distal part of the northern South China Sea in the Western Pacific region: challenge on the present-day models for the passive margins. Mar Pet Geol 93:166–181

Lester R, Lavier LL, McIntosh K, Van Avendonk HJA, Wu F (2012) Active extension in Taiwan's precollision zone: a new model of plate bending in continental crust. Geology 40(9):831–834
Li Z, Li X (2007) Formation of the 1300-km-wide intracontinental orogen and postorogenic magmatic province in Mesozoic South China: a flat-slab subduction model. Geology 35(2):179–182
Li C et al (2008) Late Mesozoic tectonic structure and evolution along the present-day northeastern South China Sea continental margin. J Asian Earth Sci 31(4–6):546–561
Li C et al. (2014) Ages and magnetic structures of the South China Sea constrained by deep tow magnetic surveys and IODP Expedition 349. Geochem Geophys Geosyst 15:4958–4983
Manatschal G (2004) New models for evolution of magma-poor rifted margins based on a review of data and concepts from West Iberia and the Alps. Int J Earth Sci 93(3):432–466
Manatschal G, Nievergelt P (1997) A continent-ocean transition recorded in the Err and Platta nappes (Eastern Switzerland). Eclogae Geol Helv 90:3–27
McIntosh K et al (2014) Crustal structure and inferred rifting processes in the northeast South China Sea. Mar Pet Geol 58(B):612–626
Mitchum RMJ, Vail PR, Sangree JB (1977) Seismic stratigraphy and global changes of sea-level, part 6: stratigraphic interpretation of seismic reflection patterns in depositional sequences. Geophys Res Lett. https://doi.org/10.1306/M26490C8
Mjelde R et al (2003) Crustal lineaments, distribution of lower crustal intrusives and structural evolution of the Voring Margin, NE Atlantic; new insight from wide-angle seismic models. Tectonophysics 369(3–4):199–218
Mooney WD, Laske G, Masters TG (1998) CRUST 5.1: a global crustal model at 5° × 5°. J Geophys Res Solid Earth 103(B1):727–747
Morley CK (2002) A tectonic model for the Tertiary evolution of strike-slip faults and rift basins in SE Asia. Tectonophysics 347(4):189–215
Nissen SS et al (1995) Deep penetration seismic soundings across the northern margin of the South China Sea. J Geophys Res 100(B11):22407–22422,433
O'Reilly BM, Hauser F, Jacob A, Shannon PM (1996) The lithosphere below the Rockall Trough: wide-angle seismic evidence for extensive serpentinisation. Tectonophysics 255(1–2):1–23
Pang X, Chen C, Peng D (2007) Deep-water fan system in the Pearl River Mouth basin of South China Sea and its significant on Petroleum. Science Press, Beijing (In Chinese)
Perez-Gussinye M, Reston TJ (2001) Rheological evolution during extension at nonvolcanic rifted margins: onset of serpentinization and development of detachments leading to continental breakup. J Geophys Res 106(B3):3961–3975
Posamentier HW, Vail PR (1988) Sequence stratigraphy: sequences and systems tract development. In: James DP, Leckie DA (eds) Sequences, stratigraphy, sedimentology: surface and subsurface, Memoir, vol 15, pp. 571–572
Prada M et al (2017) Crustal strain-dependent serpentinisation in the Porcupine Basin, offshore Ireland. Earth Planet Sci Lett 474:148–159
Pubellier M, Meresse F (2013) Phanerozoic growth of Asia: geodynamic processes and evolution. J Asian Earth Sci 72:118–128
Reston TJ, Morgan JP (2004) Continental geotherm and the evolution of rifted margins. Geology 32(2):133–136
Ru K, Pigott JD (1986) Episodic rifting and subsidence in the South China Sea. AAPG Bull 70(9):1136–1155
Savva D et al (2013) Seismic evidence of hyper-stretched crust and mantle exhumation offshore Vietnam. Tectonophysics 608:72–83
Sibuet J, Yeh Y, Lee C (2016) Geodynamics of the South China Sea. Tectonophysics 692(B):98–119
Sun Z, Zhou D, Zhong Z, Zeng Z, Wu S (2003) Experimental evidence for the dynamics of the formation of the Yinggehai basin, NW South China Sea. Tectonophysics 372(1–2):41–58
Sun Q et al (2017) Free gas accumulations in basal shear zones of mass-transport deposits (Pearl River Mouth Basin, South China Sea): an important geohazard on continental slope basins. Mar Pet Geol 81:17–32
Van Wagoner JC et al., 1988. An overview of the fundamentals of sequence stratigraphy and key definitions. In: Wilgus CK et al, Sea-level changes: an integrated approach: SEPM, Special Publication 42, pp. 39–46
Voss M, Jokat W (2007) Continent–ocean transition and voluminous magmatic underplating derived from P-wave velocity modelling of the East Greenland continental margin. Geophys J Roy Astron Soc 170(2):580–604
Wan K, Xia S, Cao J, Sun J, Xu H (2017) Deep seismic structure of the northeastern South China Sea: origin of a high-velocity layer in the lower crust. J Geophys Res Solid Earth 122(4):2831–2858
Wang P, Prell WL, Blum P, Party SS (2000) Proceedings of ocean drilling program, initial report, vol. 184, Ocean Drill. Program, College Station, Tex
Wang TK, Chen MK, Lee CS, Xia K (2006) Seismic imaging of the transitional crust across the northeastern margin of the South China Sea. Tectonophysics 412(3–4):237–254
Whitmarsh RB, White RS (1996) The ocean-continent boundary off the western continental margin of Iberia: crustal structure west of Galicia Bank. Geophys J Roy Astron Soc 103(2):509–531
Yan P, Di Z, Zhaoshu L (2001) A crustal structure profile across the northern continental margin of the South China Sea. Tectonophysics 338(1):1–21
Zhao M et al (2010) Seismic structure in the northeastern South China Sea: S-wave velocity and Vp/Vs ratios derived from three-component OBS data. Tectonophysics 480(1–4):183–197
Zhao Y, Ren J, Pang X, Yang L, Zheng J (2018) Structural style, formation of low angle normal fault and its controls on the evolution of Baiyun Rift, northern margin of the South China Sea. Mar Pet Geol 89:687–700
Zhou D et al (2008) Mesozoic paleogeography and tectonic evolution of South China Sea and adjacent areas in the context of Tethyan and Paleo Pacific interconnections. Island Arc 17(2):186–207